INTERNATIONAL JOURNAL OF
NUMERICAL ANALYSIS AND MODELING
Volume 13, Number 5, Pages 782–801

WEIGHTED HARMONIC AND COMPLEX GINZBURG-LANDAU EQUATIONS FOR GRAY VALUE IMAGE INPAINTING

ZAKARIA BELHACHMI, MOEZ KALLEL, MAHER MOAKHER, AND ANIS THELJANI

(Communicated by Jie Shen)

Abstract. We consider two second-order variational models in the image inpainting problems. The aim is to obtain in the restored region some fine features of the initial image, e.g. corners, edges, ... The first model is a linear weighted harmonic method well suited for binary images and the second one is its extension to the complex Ginzburg-Landau equation for the inpainting of multi-gray level images. The approach that we introduce consists of constructing a family of regularized functionals and to select locally and adaptively the regularization parameters in order to capture fine geometric features of the image. The parameters selection is performed, at the discrete level, with a posteriori error indicators in the framework of the finite element method. We perform the mathematical analysis of the proposed models and show that they allows us to reconstruct accurately the edges and the corners. Finally, in order to make some comparisons with well established models, we consider the nonlinear anisotropic diffusion and we present several numerical simulations to test the efficiency of the proposed approach.

Key words. Image inpainting, inverse problems, regularization procedures, adaptive finite elements.

1. Introduction

Image inpainting (or disocclusion) refers to restoring a damaged image with missing information. This type of image processing is very important and has many applications in various fields (painted canvas, movies restoration, augmented reality, ...). In fact, many images are often scratched and damaged, and the goal in the inpainting problems is to restore deteriorated or missing parts, so that a viewer cannot distinguish them from the rest. Various mathematical and heuristic techniques were considered to address this problem, such as statistical methods [23], mathematical programing and computational geometry methods [34], we refer to the article [11] and the references therein where an exhaustive review is given for this problem and for the various approaches developed to solve it. In this article we will be concerned by the Partial Differential Equations (PDE) approach which belongs to the class of the widely used methods ([6, 12, 19, 20]). Let $\Omega \subset \mathbb{R}^d$ $(d = 2, 3)$, denotes the entire domain of a given image f, the basic idea in the PDE approach, is to fill-in the damaged region $D \subset \Omega$, where the pixels of f are altered or lost, by an interpolation from the available part in $\Omega \backslash D$. Usually, the PDE-based models are obtained from the mathematical knowledge of the properties of some differential operators, and aim to fulfill some a priori expectations and assumptions on the final solution. The diffusion operators are the mostly used to this end (e.g. the heat equation, the Cahn-Hilliard equation,...[10, 12, 15, 20, 28]). Usually such models are formulated as a constrained optimization problem:

$$\text{Minimize } R(u) \quad \text{given} \quad u = f + n \ \ in \ \ \Omega \backslash D, \tag{1}$$

Received by the editors March 12, 2015 and, in revised form, July 27, 2016.
2000 *Mathematics Subject Classification.* 65M32, 65M50, 65M22, 94A08.

where the image f is given in $\Omega\backslash D$ and n is a Gaussian noise. $R(u)$ denotes the regularizing term, mostly a semi-norm of a functional space fixed a priori to enforce some expectations on the solution (e.g. a Sobolev space H^s, Bounded Variations functions space $BV, \dots$) and u is the image to be reconstructed. The unconstrained formulation of (1) reads:

$$\alpha R(u) + \frac{1}{2}\int_\Omega \lambda_D (u-f)^2 dx, \tag{2}$$

where α is a regularization parameter and $\lambda_D = \lambda_0 \chi_{\Omega\backslash D}$ for $\lambda_0 \gg 0$, a penalization factor, and $\chi_{\Omega\backslash D}$ is the indicator function of the sub-domain $\Omega \setminus D$. These two parameters α and λ_0 are chosen in order to balance the regularization term $R(u)$ and the data fitting term.

Various methods use uniform parameters α and λ, chosen in general empirically or within the regularization theory, e.g. with Morozov's criterium when the magnitude of the noise is given [25, 31]. In many applications, this choice is not reliable and may produce the loss of some relevant features of the image such as the edges (see Fig:1). Therefore, based on the importance of the scale-space representation of

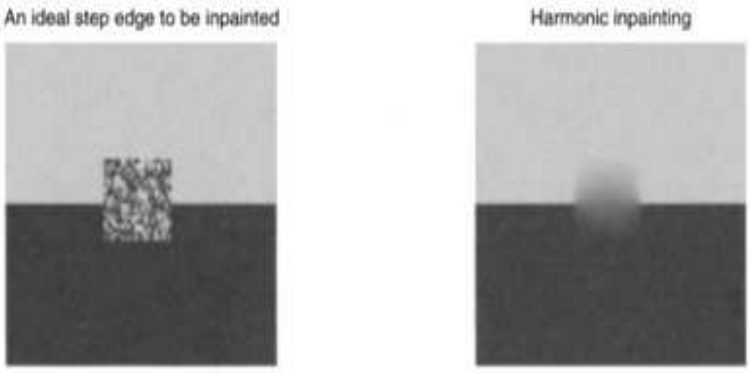

FIGURE 1. Harmonic inpainting (T. Chan and J. Shen [19]).

the image, spatially varying choices of the parameter α were proposed in the literature. We mention as an example the variant of the total variation (TV) functional, considered by D. Strong and T. Chan [36] which results in a multi-scale strategy with a uniform α updated at each scale [4]. Others strategies to choose such parameters are also developed within the statistical approach or using some a priori PDE [32] for the denoising problem. Note that the topological gradient method leads implicitly to such a choice by allowing the modification of the diffusion coefficients [5, 6].

We consider in this article a novel approach which consists of an adaptive method for the choice of such spatially varying regularization parameters. The method is well-suited for images with few textures and was successfully applied to the segmentation problems [8]. Loosely speaking, we start with a simple model (e.g. linear diffusion with a variable coefficient), then iteratively, an adaptive selection of the parameters based on some local information on the gradient magnitude is performed. The gradient information are available at the discrete level from the computed solution, thus the process is completely an a posteriori method without any reference to the continuous solution of (2). This amounts to change dynamically the reconstruction model in order to capture accurately the fine geometric structures

of the image. This approach was introduced by Hecht and Belhachmi in [9] for the optic flow estimation problem, where it was demonstrated to have several attractive features such as: the efficiency (e.g. the cost of computations, best representation of the solution,...) as well as a good edge-preserving property. Moreover, it was proven in [8] that it allows one to approximate, in the Γ-convergence sense [14], the Mumford-Shah functional (see [8, 17, 18]) although formally the continuous model remains linear (with respect to the primary variable).

The article is organized as follows: In Section 2, we introduce a weighted regularizing functional to obtain the suitable modified version of the harmonic model and we establish its properties. In Section 3, we introduce the discrete framework of the method and we make a selective diffusion, controlled by suitable error indicators. Using ([8, 17, 18])), we perform the Γ-convergence analysis of the method. We also modify the adaptive strategy in the non damaged regions in order to improve the fitting to the data term which allows us to handle simultaneously the inpainting task and the denoising of the available part of the input image. In section 4, we extend such an approach from second order linear diffusion to the complex-Ginzburg-Landau energy which is known, at least numerically, to enhance the contrast in inpainting problems and is well suited for multi-gray level images [3, 26]. We present several numerical simulations to show the performances of the method for the considered models. We also make some comparisons with the nonlinear anisotropic diffusion method which belongs to the well established techniques in the image inpainting [38].

2. Weighted harmonic inpainting

We assume that the domain Ω is partitioned into a finite number of disjoint subdomains Ω_i, $i = 1, \ldots, I$, and we consider a function α which is scalar, piecewise constant in Ω and such that

$$\alpha = \alpha_i \quad in\ \Omega_i, \quad i = 1, \ldots, I.$$

We denote by $\alpha_m = \min_{1\le i\le I} \alpha_i$, $\alpha_M = \max_{1\le i\le I} \alpha_i$, and we assume that $\alpha_m > 0$. We consider the following linear equation:

$$\begin{cases} -\nabla.(\alpha(x)\nabla u_\alpha) + \lambda_D(u_\alpha - f) = 0, & \text{in } \Omega, \\ \partial_n u_\alpha = 0, & \text{on } \partial\Omega. \end{cases} \tag{3}$$

Remark 1. It should be emphasized here that the parameter λ_0 is intended to be large enough to penalize the constraint $u_\alpha = f$ in $\Omega \setminus D$ and (3) is equivalent to the the following transmission problem:

$$\begin{cases} -\nabla.(\alpha(x)\nabla u_\alpha) + \lambda_0(u_\alpha - f) = 0, & \text{in } \Omega\backslash\overline{D}, \\ \nabla.(\alpha(x)\nabla u_\alpha) = 0, & \text{in } D, \\ [u_\alpha] = 0, & \text{on } \partial D, \\ [\alpha\nabla u_\alpha \cdot \vec{n}] = 0, & \text{on } \partial D, \\ \partial_n u_\alpha = 0, & \text{on } \partial\Omega, \end{cases} \tag{4}$$

where $[\cdot]$ denotes the jump across ∂D.

We define the subspace $V = \{u \in H^1(\Omega); \int_D u\,dx = 0\}$. Therefore, under the previous assumptions on the function α, we have:

Proposition 1. *Let $f \in L^2(\Omega)$, then the problem (3) admits a unique weak solution u_α in V.*

Proof. Equation (3) is the optimality condition of the following minimization problem:

$$\min_{v\in V}\{F_\alpha(v)=\int_\Omega \alpha(x)|\nabla v|^2dx+\int_\Omega \lambda_D(v-f)^2dx\}. \tag{5}$$

One may check directly that F_α is convex and weakly lower semi-continuous in $H^1(\Omega)$. For $u\in V$, we have:

$$F_\alpha(u)\geq \alpha_m\int_{\Omega\setminus\overline{D}}|\nabla u|^2\,dx+\lambda_0\int_{\Omega\setminus\overline{D}}(u-f)^2\,dx+\alpha_m\int_D|\nabla u|^2\,dx.$$

Using the previous inequality and applying the Poincaré-Wirtinger inequality in D, we get:

$$F_\alpha(u)\geq c\|u\|^2_{H^1(\Omega)},$$

where the constant c is dependent on α_m, λ_0 and the geometry of D. which implies that F_α is coercive. Thus, the functional F_α admits a minimizer $u_\alpha\in V$. The uniqueness is guaranteed by the strict convexity of F_α. □

The weak formulation of (3) reads:

$$\begin{cases}\text{find } u_\alpha\in V, \text{ such that:}\\ a_\alpha(u_\alpha,v)=l(v),\ \forall v\in V,\end{cases} \tag{6}$$

where

$$\begin{cases} a_\alpha(u,v)=\displaystyle\int_\Omega \alpha(x)\nabla u\cdot\nabla v dx+\int_\Omega\lambda_D uvdx,\\ l(v)=\displaystyle\int_\Omega\lambda_D fvdx.\end{cases} \tag{7}$$

The equivalence of the problems (6) and (5) follows by standard arguments. Note that if Ω is Lipschitz-continuous, $f\in L^2(\Omega)$ and $\lambda_D\in L^{+\infty}(\Omega)$, the following regularity result holds [7, Proposition 2.5]

Proposition 2. *There exists a constant c only depending on the geometry of Ω, such that a weak solution u_α of problem (6) belongs to $H^{s+1}(\Omega)$, for all real numbers $s<s_0$, where s_0 is given by*

$$s_0=\min\left\{\frac{1}{2},c|\log(1-\frac{\alpha_m}{\alpha_M})|\right\}.$$

Remark 2. This result reminds us that even non-smooth the solution of (6) is $H^1(\Omega)$ and therefore admits no jump inside Ω. Nevertheless, our approach consists in decreasing the diffusion coefficient α in high gradient zones (formally to zero) encouraging possible jumps in these areas.

2.1. Discrete problem and adaptivity. We assume that the domain Ω is polygonal. We consider a regular family of triangulations $\mathcal{T}_h$ made of elements which are triangles (or quadrilaterals) with a maximum size h, satisfying the usual admissibility assumptions, i.e., the intersection of two different elements is either empty, a vertex, or a whole edge. For $h>0$, we introduce the following discrete space:

$$X_h=\left\{v_h\in C(\overline{\Omega})|\forall K\in\mathcal{T}_h, v_h|_K\in P_1(K)\right\}\cap V,$$

and the following notations: for u_h, $v_h\in X_h$:

$$\begin{cases} a_{\alpha,h}(u_h,v_h)=\displaystyle\int_\Omega\alpha_h(x)\nabla u_h\cdot\nabla v_h dx+\int_\Omega\lambda_D u_hv_hdx,\\ l_h(v)=\displaystyle\int_\Omega\lambda_D f_hv_h\,dx,\end{cases} \tag{8}$$

where f_h is a finite element approximation of f associated with $\mathcal{T}_h$. The discrete problem leads to:

$$\begin{cases} \text{find } u_{\alpha,h} \in X_h, \text{ such that:} \\ a_{\alpha,h}(u_{\alpha,h}, v_h) = l_h(v_h), \ \forall v_h \in X_h. \end{cases} \tag{9}$$

Proposition 3. *There exists a unique solution $u_{\alpha,h}$ in X_h of the discrete problem (9).*

Proof. The proof can be carried out by applying the Lax-Milgram Lemma. Furthermore, we have following finite element error:

$$\|u_\alpha - u_{\alpha,h}\|_V \approx O(h).$$

□

Remark 3. We do not impose any compatibility of the mesh with the "partition" $D \cup (\Omega \setminus \overline{D})$. We are given a regular mesh over Ω similarly to the fictitious domain methods.

2.2. Adaptive local choice of α. For an element $K \in \mathcal{T}_h$, we denote by $\mathcal{E}_K$ the set of its edges not contained in the boundary $\partial\Omega$. The union of all $\mathcal{E}_K$, $K \in \mathcal{T}_h$ is denoted by $\mathcal{E}_h$. With each edge $e \in \mathcal{E}_h$, we associate a unit vector n_e normal to e and we denote by $[\phi]_e$ the jump of the piecewise continuous function ϕ across e in the direction n_e. For each $K \in \mathcal{T}_h$, we denote by h_K the diameter of K and we denote by h_e the length of e, $e \in \mathcal{E}_K$ and f_h a finite element approximation of f. We define the residual error indicator as follows: for each element $K \in \mathcal{T}_h$, we set:

$$\eta_K = \alpha_K^{-\frac{1}{2}} h_K ||\lambda_D^{\frac{1}{2}}(u_{\alpha,h} - f_h) + \alpha_h \Delta u_{\alpha,h}||_{L^2(K)} + \tfrac{1}{2} \sum_{e \in \mathcal{E}_K} \alpha_e^{-\frac{t}{2}} h_e^{\frac{1}{2}} ||[\alpha \nabla u_{\alpha,h} \cdot n_e]_e||_{L^2(e)},$$

where $\alpha_e = \max(\alpha_{K1}, \alpha_{K2})$, K_1 and K_2 being the two elements adjacent to e. On the triangulation $\mathcal{T}_h$, we compute the solution $u_{\alpha,h}$ of problem (9) and the corresponding error indicator which is well know to be equivalent to the H^1-norm of the finite element error (see [8] for details) and allows mostly mesh adaptation. η_K gives the error distribution of the computation of $u_{\alpha,h}$, and includes information about edges in the following term:

$$\tfrac{1}{2} \sum_{e \in \mathcal{E}_K} \alpha_e^{-\frac{1}{2}} h_e^{\frac{1}{2}} ||[\alpha \nabla u_{\alpha,h} \cdot n_e]_e||_{L^2(e)}. \tag{10}$$

In fact, the edges in the image are characterized by the brightness changes (large gradients). Therefore the quantity (10) acts as a measure locating regions of edges and will be used next to control the parameter α.

Remark 4. The gradient can represent the change in gray level and his magnitude provides information about the strength of the edge. Since all error indicators are (mainly) equivalent [37], we may change the error indicator η_K by the following local energy:

$$\eta'_K = \alpha_K^{\frac{1}{2}} h_K^{\frac{1}{2}} ||\nabla u_{\alpha,h}||_{L^2(K)}, \tag{11}$$

which might be well suited in the adaptation steps and behaves like the residual error indicator.

Adaptive strategy. We control the diffusion process by following the adaptive algorithm: Given the initial grid $\mathcal{T}_h^0$ in Ω, we:

(1) Compute $u_{\alpha^0,h}$ solution of the problem (3) on $\mathcal{T}_h^0$ with a large constant $\alpha = \alpha^0$.
(2) We build an adapted isotropic mesh $\mathcal{T}_h^1$ (in the sense of the finite element method, i.e. with respect to the parameter h) with the metric error indicator ([8]).
(3) We perform an automatic local choice of $\alpha(x)$ on $\mathcal{T}_h^1$ to obtain a new function $\alpha^1(x)$ in D.
(4) Go to step (1) and compute $u_{\alpha^1,h}$ on $\mathcal{T}_h^1$.

During the adaptation, we use the following formula: for each triangle K

$$\alpha_K^{k+1} = max\left(\frac{\alpha_K^k}{1+\kappa * \left(\left(\frac{\eta_K}{||\eta||_\infty}\right) - 0.1\right)^+}, \alpha_{thr}\right), \tag{12}$$

where α_{trh} is a threshold parameter and κ is a coefficient chosen to control the rate of decrease of α, $(u^+) = \max(u, 0)$. Here η is the piecewise-constant function such that $\eta|_K = \eta_k,\ \forall K \in \mathcal{T}_h^1$.

The formula (12) means that in the regions of high gradients, one decreases the values of α. Actually, if the error indicator deviates more than 10% from its mean value, then there is a large error which indicates that the element contains a part of the singular set of u. Therefore, decreasing α (nearly as a geometric sequence with the iteration number) produces an edge location.

The adaptive algorithm consists of two steps. First, given α, we solve a linear equation (3) and build an adapted isotropic mesh $\mathcal{T}_h$. The adapted mesh is obtained by coarsening the initial grid in the homogeneous regions and by refinement to obtain smaller elements 'close' to the jump set of u. Second, we update the value of α in every element K of $\mathcal{T}_h$ in accordance with the formula (12).

2.3. Γ-convergence analysis of the adaptive algorithm. A Γ-convergence study of the adaptive strategy is performed in [8] for the optical flow problems. Analyzing this strategy, the authors proved that it is equivalent to the adaptive algorithm introduced for denoising, by Chambolle-Dal Maso in [18] and Chambolle-Bourdin in [17] where a similar method for the numerical discrete approximation of the Mumford-Shah energy was proposed. They proved that this method, based on finite element discretization and adaptive mesh strategy, is a good approximation in the Γ-convergence sense [14] of the Mumford-Shah energy. We briefly recall the results and the numerical approximation of this method. For a fixed angle $0 < \theta_0 \leq \pi/3$, a constant $c \geq 6$, and for $\epsilon > 0$, we denote $\mathcal{T}_\epsilon(\Omega) = \mathcal{T}_\epsilon(\Omega; \theta_0; c)$ the set of all triangulations of Ω whose triangles K have the following characteristics:

i) The length of all three edges of K is between ϵ and ϵc.
ii) The three angles of K are greater than or equal to θ_0.

Let $V_\epsilon(\Omega)$ the set of all continuous functions $u : \Omega \longrightarrow \mathbb{R}$ such that u is affine on any triangle K of a triangulation $\mathbb{T} \in \mathcal{T}_\epsilon(\Omega)$ and for a given u, $\mathcal{T}_\epsilon(u) \subset \mathcal{T}_\epsilon(\Omega)$ is the set of all triangulations adapted to the function u, i.e., such that u is piecewise affine on $\mathbb{T}$. They introduce a non-decreasing continuous function $g : [0, +\infty) \longrightarrow [0, +\infty)$ such that:

$$\lim_{t\to 0} \frac{g(t)}{t} = 1,\ \lim_{t\to+\infty} g(t) = g_\infty.$$

For any $u \in L^p(\Omega), (p \geq 1)$ and $\mathbb{T} \in \mathcal{T}_\epsilon(\Omega)$, the authors in [18] introduced the following minimization problem:

$$G_\epsilon(u) = \min_{\mathbb{T}\in\mathcal{T}_\epsilon(\Omega)} \tilde{G}_\epsilon(u, \mathbb{T}), \tag{13}$$

where

$$\tilde{G}_\epsilon(u, \mathbb{T}) = \begin{cases} \sum_{K\in\mathbb{T}} |K \cap \Omega| \dfrac{1}{h_K} g(h_K |\nabla u|^2), & u \in V_\epsilon(\Omega), \mathbb{T} \in \mathcal{T}_\epsilon(\Omega), \\ +\infty, & \text{Otherwise.} \end{cases}$$

For ϵ going to zero and provided θ_0 is less than some $\Theta > 0$, they proved that the energy G_ϵ Γ-converges to the Mumford-Shah functional:

$$G(u) = \begin{cases} \int_\Omega |\nabla u|^2 \, dx + g_\infty \mathcal{H}^1(S_u), & u \in L^2(\Omega) \cap GSBV(\Omega), \\ +\infty, & u \in L^2(\Omega) \backslash GSBV(\Omega), \end{cases}$$

where $\mathcal{H}^1$ is the 1-dimensional Hausdorff measure and $GSBV(\Omega)$ is the space of generalized special functions with bounded variation (see [1]). It follows from the Γ-convergence to G_ϵ [18, Theorem 2]:

Theorem 2.1. *Let $(u^\epsilon)_{\epsilon>0}$ be a family of functions such that $u^\epsilon \in V_\epsilon(\Omega)$ for all $\epsilon > 0$ and*

$$\sup_{\epsilon>0} G_\epsilon(u^\epsilon) + ||u^\epsilon||_{L^2(\Omega)} < +\infty. \tag{14}$$

Then there exists $u \in GSBV(\Omega)$ and a subsequence $(u^{\epsilon_j})_j$ converging to u, a.e. in Ω, such that:

$$G(u) \leq \liminf G_{\epsilon_j}(u^{\epsilon_j}),$$

and, if for each ϵ, u^ϵ is a solution of:

$$\min_v G_\epsilon(v) + \int_\Omega \lambda_D |v - f|^2 dx, \tag{15}$$

then the limit u solves:

$$\min_v G(v) + \int_\Omega \lambda_D |v - f|^2 dx, \tag{16}$$

and u^{ϵ_j} converges strongly to u.

We suppose that the function g is concave and differentiable and that $g(0) = 0$. Thus, extending g with the value $-\infty$ on $]-\infty, 0]$, $-g$ is convex and lower semi-continuous. We have (see [24]),

$$-g(t) = \sup_{v\in\mathbb{R}} -\psi(-v) = \inf_{v\in\mathbb{R}} tv + \psi(v),$$

where $\psi(-v) = \sup_{t\in\mathbb{R}} tv - (-g)(t) = (-g)^*(v)$ is the Legendre-Fenchel conjugate of $(-g)$. The first supremum is achieved at v such that $t \in \partial(-g)^*(v)$ which is equivalent to $v \in \partial(-g)(t)$. Since $\partial(-g)(t)$ is given as: $\{-g'(t)\}$ if $t > 0$ and $]-\infty, -1]$ if $t = 0$, we deduce that the sup is reached at some $v \in [-1, 0]$ (in fact, for $t = 0$, we check that $(g)^*(-1) = 0$ and the supremum is achieved at $v = -1$), we obtain:

$$g(t) = \min_{v\in[0,1]} tv + \psi(v),$$

and the minimum is achieved for $v = g'(t)$ and therefore, for a given triangulation $\mathbb{T}_\epsilon$, the minimization of G_ϵ is then equivalent to minimize the following functional:

$$G'_\epsilon(u, v, \mathbb{T}_\epsilon) = \sum_{K\in\mathbb{T}_\epsilon} |K \cap \Omega| \frac{1}{h_K} (v_K |\nabla u|^2 + \frac{\psi(v_K)}{h_K}),$$

over all $u \in V_\epsilon(\Omega)$ and $v = (v_K)_{K\in\mathcal{T}_\epsilon}$, piecewise constant on each $K \in \mathbb{T}_\epsilon$. For a fixed u, the minimizer over each v is explicitly given by:

$$v_K = g'(h_K|\nabla u|^2), \tag{17}$$

and the optimal u for fixed v solves an elliptic equation. The adaptive algorithm minimizes G' with $v = \alpha$.

Remark 5.

- Given a function α, the computation of the minimization problem with respect to u is simple and very fast because after each adaptation step, one solves a linear problem with the number of nodes of the mesh which decreases.
- For computational reasons, we have chosen the formula (12) to update the diffusion function α (which is similar to the choice $g(t) = \lambda \min(t, \mu)$ for given constants λ and μ). This allows for stable computations, other possible choices to update α are possible. In [17], the authors considered a smooth function $g(t) = M \arctan(\frac{t}{M})$, for $M > 0$ which leads according to the formula (16) to the diffusion function
$$\alpha_K = \frac{1}{1 + (h_K|\nabla u|)^2}.$$
- It may be noticed that the parameter α acts as a "phase field function" and plays a role similar to the z-field in the Ambrosio-Tortorelli approximation [2] method for the Mumford-Shah energy. However, the edges obtained in our case seems sharper and their "thickness" is controlled by the refinement strategy. This behavior of α is shown in Fig: 9 in the numerical examples.

2.4. The inpainting with the image restoration. Numerical evidences show that there is a strong connection between the noise removal in the available part of the initial image and the inpainting process. To overcome this sensitivity to the noise, a natural idea is to perform simultaneously the denoising in $\Omega \setminus \overline{D}$ and the fill-in in D. The two steps are coherently integrated in the method. Thus, we replace now the previous constant λ_0 with a spatially varying function $\lambda(x)$ and we will select locally it values in order to decide whether we should encourage the penalization (by increasing λ) or not. As mentioned in the remark (1), the residual error indicator splits as for the transmission problem:

(18)
$$\begin{cases} \text{If } K \cap \Omega\setminus\overline{D} \neq \emptyset, \text{ we have :} \\ \eta_K = \alpha_K^{-\frac{1}{2}} h_K ||\lambda_K^{\frac{1}{2}}(u_{\alpha,h} - f_h) + \alpha_h \Delta u_{\alpha,h}||_{L^2(K)} \\ \qquad\qquad + \frac{1}{2}\sum_{e\in\mathcal{E}_K} \alpha_e^{-\frac{1}{2}} h_e^{\frac{1}{2}} |||[\alpha_e \nabla u_{\alpha,h} \cdot n_e]|||_{L^2(e)}, \\ \text{and if } K \cap \Omega \setminus \overline{D} = \emptyset, \text{ we have :} \\ \eta_K = \alpha_K^{-\frac{1}{2}} h_K ||\alpha_K \Delta u_{\alpha,h}||_{L^2(K)} + \frac{1}{2}\sum_{e\in\mathcal{E}_K} \alpha_e^{-\frac{1}{2}} h_e^{\frac{1}{2}} |||[\alpha_e \nabla u_{\alpha,h} \cdot n_e]|||_{L^2(e)}. \end{cases}$$

For an element $K \subset \Omega\setminus\overline{D}$, the error indicator contains a supplementary term, i.e.

$$E_K = \alpha_K^{-\frac{1}{2}} h_K ||\lambda_K^{\frac{1}{2}}(u_{\alpha,h} - f_h) + \alpha_h \Delta u_{\alpha,h}||_{L^2(K)}, \tag{19}$$

where λ_K is the constant value of λ in the element K. In this term the parameters are competing and finding a balance is not obvious. Since our purpose is to make a noise filtering we choose to keep α fixed and to adjust only λ. In fact, starting with a large value of α_0 in the previous algorithm will smooth the input image f in $\Omega\setminus\overline{D}$

at the first iterations which produces some undesirable blurring in this part of the domain. Thus, in $\Omega \setminus \overline{D}$, we keep such α constant and increase λ to enhance the fidelity term. In D, the process is unchanged. This calls for a slight modification of the previous algorithm. We start with a constant value λ_0. If $K \cap \Omega \backslash \overline{D} \neq \emptyset$, then we update λ as follows:

$$\lambda_K^{k+1} = \min\{\lambda_K^k * \left(1 + \kappa * \left(\left(\frac{E_K}{||E||_\infty}\right) - 0.1\right)^+\right), \lambda_0\}, \tag{20}$$

The explanation of this formula is identical to that of α previously, that is if the error indicator is 10% larger than the mean value, the fidelity constraint should be enforced by increasing λ at that location.

3. Adaptive strategy in the complex Ginzburg-Landau equation

We extend such an approach from the linear diffusion to the complex-Ginzburg-Landau energy. This model was originally developed by Ginzburg & Landau in [29] to describe phase separation and it is given by:

$$-\Delta u + \frac{W'(u)}{\epsilon^2} = 0, \tag{21}$$

where $u : \Omega \longrightarrow \mathbb{C}$, ϵ is a small positive parameter and $W(u) = (1-|u|^2)^2$. It is the Euler-Lagrange equation associated to the minimization of the following energy:

$$\frac{1}{2}\int_\Omega |\nabla u|^2 dx + \int_\Omega \frac{W(u)}{2\epsilon^2} dx. \tag{22}$$

For digital image inpainting purposes, this equation was developed by H. Grossauer and O. Scherzer in [26]. The key advantage of this model is that its solutions are known to produce effects like vortices and shockwaves of the phase when $\epsilon \longrightarrow 0$ and the solution reveals high contrast in the inpainting domain, which makes it well suited for multiple gray level images.

The real Ginzburg-Landau equation (21) is appropriate only for two-scale images, while the minima of the potential W are attained in the sphere $|u| = 1$. For gray-scale images, we follow the same methodology of Grossauer and Scherzer in [26]. We rescale the intensity of the input image $f(x)$ to the interval $[-1, 1]$. Then f is identified with the real part of the complex valued function $f_{re} : \Omega \longrightarrow \mathbb{C}$. We then define:

$$\begin{cases} f = f_{re} + i f_{im}, \text{ where:} \\ f_{re} = f_0 (\text{the initial damaged image}), \\ f_{im} = \sqrt{1 - f_0^2}. \end{cases} \tag{23}$$

By this choice, the complex valued solution u will also have an absolute value equal to 1 but our inpainting f_{re} may contain any value in the interval $[-1, 1]$. The aim is to minimize the following Ginzburg-Landau energy:

$$F_\epsilon(u) = \int_\Omega \frac{\alpha(x)}{2} |\nabla u|^2 dx + \int_\Omega \frac{W(u)}{2\epsilon^2} dx + \frac{1}{2}\int_\Omega \lambda_D (u - f)^2, \tag{24}$$

over $V = \{u \in H^1(\Omega, \mathbb{C}); \int_D u\, dx = 0\}$ and where $H^1(\Omega, \mathbb{C})$ is the space of complex functions equipped with the norm:

$$||u||_1^2 = \int_\Omega u\overline{u} dx + \int_\Omega \nabla u \cdot \overline{\nabla u} dx.$$

For the sake of clarity, we omit the ϵ dependence for the minimizers of F_ϵ. Then, u_α satisfies the following Euler-Lagrange equation:

$$\begin{cases} -\nabla.[\alpha(x)\nabla u_\alpha] + \dfrac{1}{\epsilon^2}u_\alpha(|u|_\alpha^2 - 1) + \lambda_D(u_\alpha - f) = 0, & \text{in } \Omega, \\ \alpha(x)\partial_n u_\alpha = 0, & \text{on } \partial\Omega. \end{cases} \tag{25}$$

It is readily checked (see [13] for details).

Proposition 4. *The functional (24) admits a minimizer u_α in V. Moreover, u_α is a weak solution of (25) and $|u_\alpha| \leq 1$.*

Evolution equation and discretization. We consider the associated evolution problem:

$$\frac{\partial u_\alpha}{\partial t} - \nabla.[\alpha(x)\nabla u_\alpha] + \frac{W'(u_\alpha)}{\epsilon^2} + \lambda_D(u_\alpha - f) = 0, \quad \text{in } \mathbb{R}^+ \times \Omega, \tag{26}$$

with homogeneous Neumann boundary conditions and the initial time condition $u_\alpha(t = 0, x) = f(x)\ \forall x \in \Omega$. We assume without loss of generality that $\int_\Omega f = 0$ and $\|f\| \leq 1$. The weak solution of (26) solves: find $u \in L^2(0, T; V)$ such that

$$\int_\Omega \frac{\partial u_\alpha}{\partial t}\phi dx + \int_\Omega \alpha(x)\nabla u_\alpha \nabla\phi dx + \int_\Omega \frac{W'(u_\alpha)}{\epsilon^2}\phi dx + \int_\Omega \lambda_D(u_\alpha - f)\phi dx = 0 \quad \forall \phi \in H^1(\Omega, \mathbb{C}).$$

Time discretization. We use the linearly implicit Euler scheme: given u_α^n, find $u_\alpha^{n+1} \in H^1(\Omega, \mathbb{C})$ such that

$$\int_\Omega \frac{u_\alpha^{n+1} - u_\alpha^n}{\delta t}\phi dx + \int_\Omega \alpha_h \nabla u_\alpha^{n+1}\nabla\phi dx + \frac{1}{\epsilon^2}\int_\Omega (|u_\alpha^n|^2 - 1)u_\alpha^{n+1}\phi dx + \int_\Omega \lambda_D(u_\alpha^{n+1} - f)\phi dx = 0 \ \ \forall \phi \in H^1(\Omega, \mathbb{C}).$$

4. Comparison with the nonlinear diffusion methods

For the sake of completeness, we will make a comparison with the nonlinear diffusion method [38] that we recall now. The earliest model considered is the so-called nonlinear isotropic diffusion by Perona and Malik [33]. The diffusion coefficient was a nondecreasing function g of $|\nabla u|^2$ with $g(0) = 1$, $g(s) > 0$ and $\lim_{s \longrightarrow +\infty} g(s) = 0$. The method was extended to the anisotropic case by J. Weickert in [38] who replaced the scalar diffusion function g with a diffusion tensor D depending on $|\nabla u_\sigma|^2$, where u_σ is a smoothed version of u (convolution with a smoothing kernel). The diffusion is adjusted according to the directional information contained in the image structure. In our case, the anisotropic model may be written as follows:

$$\begin{cases} \dfrac{\partial u}{\partial t} - \nabla.[D(\nabla u_\sigma)\nabla u] + \lambda_D(u - f) = 0, & \text{in } \mathbb{R}^+ \times \Omega, \\ u(x, 0) = f, & \text{in } \Omega, \\ < D(\nabla u_\sigma)\nabla u \cdot n >= 0, & \text{on } \mathbb{R}^+ \times \partial\Omega. \end{cases} \tag{27}$$

Following [38], let $\{v_1, ..., v_d\}$, be an orthonormal basis of $\mathbb{R}^d$ $(d = 2, 3)$ such that $v_1 || \nabla u_\sigma$. The matrix D is symmetric, positive definite and $\{v_1, ..., v_d\}$ represent its eigenvectors with corresponding eigenvalues $\{\Lambda_1, ..., \Lambda_d\}$. Then we have:

$$D(\nabla u_\sigma) = (v_1|...|v_d)\text{diag}(\Lambda_1, ..., \Lambda_d)(v_1|...|v_d)^T. \tag{28}$$

These eigenvalues are chosen to be functions of $|\nabla u_\sigma|$ in order to obtain a diffusion tensor adapted to the local structure of the image (i.e., homogeneous area or edges). Let $g \in C^\infty([0,\infty),(0,1])$ be a Lipschitz continuous scalar function which is represented in $[0,+\infty)$ by a convergent power series as follows:

$$g(s) = \sum_{k=0}^{\infty} a_k s^k,$$

and we consider the tensor product $J_0(\nabla u_\sigma) = \nabla u_\sigma \otimes \nabla u_\sigma$. For the two dimensional case, the matrix:

$$D(\nabla u_\sigma) = g(\sqrt{|J_0(\nabla u_\sigma)|}) = \sum_{k=0}^{\infty} a_k (\sqrt{|J_0(\nabla u_\sigma)|})^k, \tag{29}$$

defines a diffusion tensor with an orthonormal system of eigenvectors (v_1, v_2) where:

$$v_1 = \begin{pmatrix} v_1^1 \\ v_1^2 \end{pmatrix} = \frac{\nabla u_\sigma}{|\nabla u_\sigma|} \quad \text{and} \quad v_2 = \begin{pmatrix} v_1^2 \\ -v_1^1 \end{pmatrix}.$$

The choice that prevents the diffusion over the edge lead to the matrix D:

$$D = \begin{pmatrix} | & | \\ v_1 & v_2 \\ | & | \end{pmatrix} \begin{pmatrix} \Lambda_1 & 0 \\ 0 & \Lambda_2 \end{pmatrix} \begin{pmatrix} | & | \\ v_1 & v_2 \\ | & | \end{pmatrix}^T.$$

Different classes of anisotropic models and diffusivity functions "g" may be used (see [21, 22, 32, 38]). In this article we choose the following function:

$$g(s) = \frac{1}{\sqrt{\epsilon + s^2/R^2}}, \tag{30}$$

where R and ϵ are a contrast and a resolution parameters, respectively. The variational formulation of problem (27) reads:

$$\begin{cases} \text{Find } u \in C((0,T);V), \text{ such that:} \\ \displaystyle\int_\Omega \frac{\partial u}{\partial t} v\, dx + a(u;u,v) = l(v), \ \forall v \in V, \end{cases} \tag{31}$$

where

$$\begin{cases} a(w;u,v) = \displaystyle\int_\Omega D(\nabla w_\sigma)\nabla u \cdot \nabla v dx + \int_\Omega \lambda_D uv dx, \\ l(v) = \displaystyle\int_\Omega \lambda_D f v dx. \end{cases} \tag{32}$$

Iterative scheme: To find the solution u of the nonlinear problem (27), we start from an initial guess u_0 and we use the explicit Euler scheme with $\dfrac{\partial u}{\partial t}$ replaced by $\dfrac{u^{n+1}-u^n}{\delta t}$ (where δt is the time step). We then obtain the following semi-implicit problem:

$$\begin{cases} \text{Given } u^n, \text{find } u^{n+1} \in V, \text{ such that:} \\ \displaystyle\int_\Omega \frac{u^{n+1}-u^n}{\delta t} v\, dx + a(u^n, u^{n+1}, v) = l(v) \ \ \forall v \in V. \end{cases} \tag{33}$$

At each iteration, the bilinear form $a(u^n, u^{n+1}, v)$ is symmetric and positive definite and the problem (33) is well defined. The proof of the next proposition is a straightforward application of the analysis in [16] (see also Weickert [38]).

Proposition 5.

(i) *Let $f \in L^2(\Omega)$; then there is a unique solution $u(t,x)$ of (27), $u \in C([0,T];V) \cap L^2(0,T;V')$, V' stands for the dual of V.*
(ii) *Let $(u^n)_n$ denotes the sequence of solutions of the linearized problems (33). Then, the sequence $(u^n)_n$ converges, in $C([0,T];L^2(\Omega))$ as $n \to +\infty$, to the solution u of problem (27).*

5. Numerical examples

All the PDEs considered in this section are solved using the finite element open source software FreeFem++ [27]. In all the examples, the damaged regions are marked with red color rectangles. All the examples are for 2-D images.

Examples 1. In the first example, the task is to fill broken edges in a white strip. We display in Fig. 2 the evolution of the meshes for iterations 1, 10 and 20. one can see that the meshes are progressively sparse. The first mesh is $\mathcal{T}_0$ which is a regular grid where every pixel corresponds to a node. The harmonic inpainting without adaptation in Fig. 3 does not achieve any connectedness and produces a smooth solution u in D, blurring the edges. At the contrary, with the adaptive algorithm the edges of the strip are well captured.

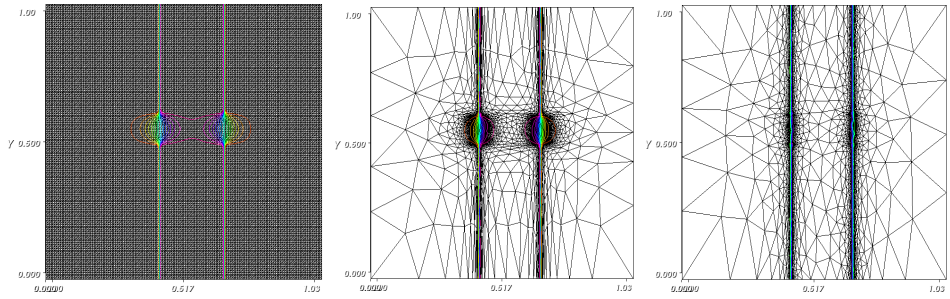

FIGURE 2. The mesh at iterations 1, 10 and 20, respectively.

FIGURE 3. From left to right: Damaged, Harmonic and Harmonic & adaptation images, respectively.

Examples 2. In the second example, we have chosen a 220×250 gray-scale image containing some edges and jumps. The damaged regions are numbered (see Fig. 4). We show in Fig. 5 the results obtained using the total variation (left) and the harmonic models without adaptation (middle), and with the adaptation, using the error indicator η_K (right). Note that the total variation is approximated here with $\sqrt{\epsilon + |\nabla u|^2}$ ($\epsilon = 0.001$).

In Fig. 6, we display the inpainted images using the weighted harmonic model where we adapt with the error indicator η'_k (left), the Ginzburg-Landau with adaptation (middle) and the anisotropic model (right). We have performed the adaptation with the two residual error indicators of Section 2. In both cases, we initialized the algorithm by a large value of $\alpha = \alpha_0 = 50$ and we performed 20 iterations for the error indicator η_K and 40 iterations for η'_K. We give in Fig. 9 the two error indicators η_K and η'_K at the final iteration of the algorithm. We note that numerically, the error indicator η'_K performs better for these examples as it is computed in the element K, rather than from the jumps on the edges which is less stable for computations.
In addition, we emphasize that the adaptive method, both the weighted harmonic and the the Ginzburg-Landau equation, gives visually comparable results to those obtained using the anisotropic nonlinear model. The dissimilarities are only seen by zooming (so at few pixels scale).
We present in Fig. 10 and Fig. 11 the evolution of the mesh for some iterations (0, 2, 10 and 20) where we used η'_K as an error indicator. The number of elements decreases at the first iterations and produces sparse solutions requiring few degrees of freedom in the homogeneous zones. This is shown by the curve in Fig. 12 where we presented the degrees of freedom (right) and the L^2-error $ER = ||u^k_\alpha - u_{exact}||$ between the restored and the exact image (left), in a semi-log scale, as a function of the number of iterations. Note that the gain in term of the reduction of degrees of freedom depends also on the size of the edges set and may be enhanced by more unrefinement in the homogeneous areas (see [8]).

In the numerical experiment in Fig. 13 , the aim is to remove the foreground text in the input image. We initialized the algorithm with a large value of $\alpha = 50$ and we performed 10 iterations of the adaptive algorithm. The text has been successfully removed and the restored image is close to the original one. We display the difference between the original and the restored images at iterations 1 and 10 respectively and we give in Fig. 14 a zoom caption (the resolution is degraded in the initial image however the "blurring" produced by the adaptive method$--\alpha > 0--$is discernible at this scale).

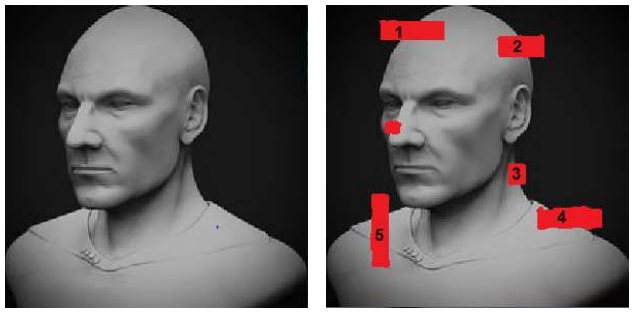

FIGURE 4. Original and damaged images.

Examples 3. We present in Fig. 15 the result for simultaneous image inpainting and denoising. The input image f is corrupted by a Gaussian noise in the region $\Omega \backslash D$. We started the computation with $\alpha = 50$ in the entire image domain which produces a blurring of the edges at the first iterations. However, the simultaneous adaptive choice of α and λ allows us to recover the edges. We present the evolution

FIGURE 5. From left to right: restored images using total variation, harmonic and harmonic & adaptation (indicator η_K).

FIGURE 6. From left to right: restored images using Harmonic & adaptation (indicator η'_K), Complex Ginzburg-Landau and anisotropic diffusion.

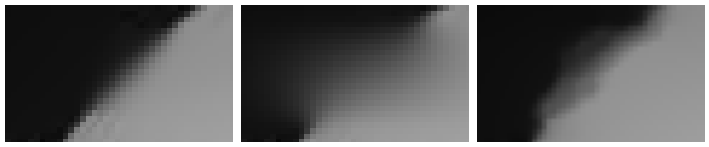

FIGURE 7. Zoom on region 1 (40×25 Pixels): Total variation - Harmonic - Harmonic & adaptation (indicator η_K).

FIGURE 8. Zoom on region 1 (40×25 Pixels): Harmonic (indicator η'_K) - Complex Ginzburg-Landau - Anisotropic.

of the restored image for iterations 5 and 20. In the 5th iteration (middle), the image is smoothed even in the regions where the data is available. λ is increased during the process following the formula (20) in order to fit the data-term.

Examples 4. In Fig 17 and Fig 16, we compare different methods when the damaged region contains a corner. The anisotropic nonlinear model (see the left-hand

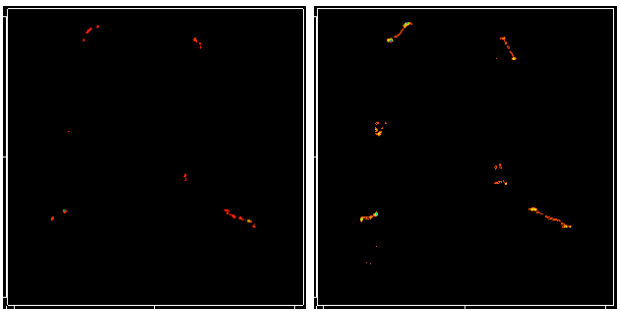

FIGURE 9. The error indicators η_K and η'_K at the convergence.

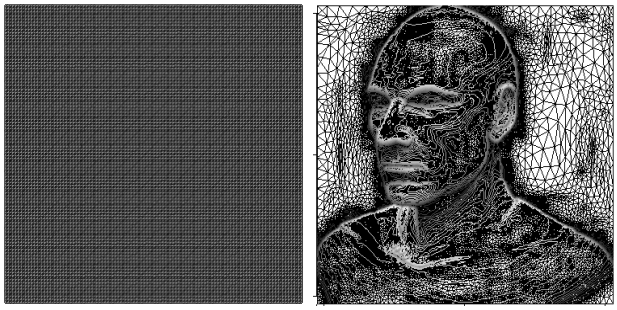

FIGURE 10. The initial mesh and the adapted one at iteration 2.

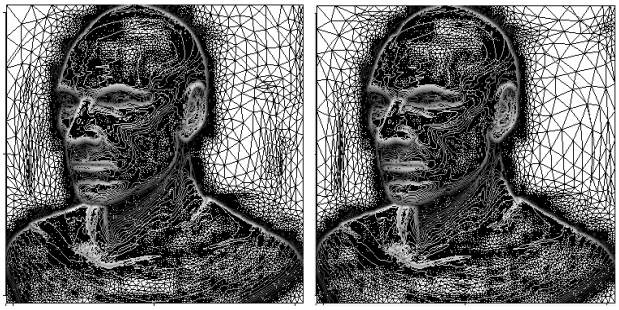

FIGURE 11. The mesh at iterations 10 and 20.

plots of Fig 17) produces well contrasted edges separating the three homogeneous areas of the inpainting domain. But, the corner itself is not well captured. The harmonic model with adaptation (see the middle plots of Fig 17), approximates better the solution near the corner (still not well captured) and the edges are improperly contrasted. In the left-hand plots of Fig 17, we display the solution of the complex Ginzburg-Landau equation with the adaptation. First, the complexification allows us to diffuse more than two colors (0 and 1). Second, this model with adaptation allows us to approximate and to capture the corner (relatively to the other methods), and reveals high contrast, which is an advantage of this model compared to the other ones in this case. We display in Fig 18 the evolution of the mesh at iterations 0, 7 and 30 for the complex Ginzburg-Landau equation.

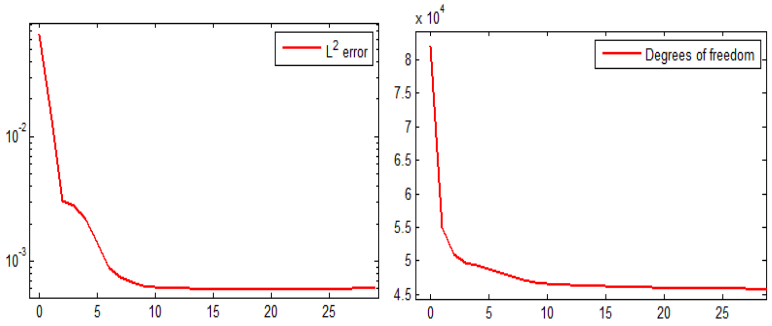

FIGURE 12. (Left:) The error $\log ER = \log ||u_\alpha^k - u_{exact}||_2$, and (Right:) the number of degrees of freedom, as functions of the iteration numbers.

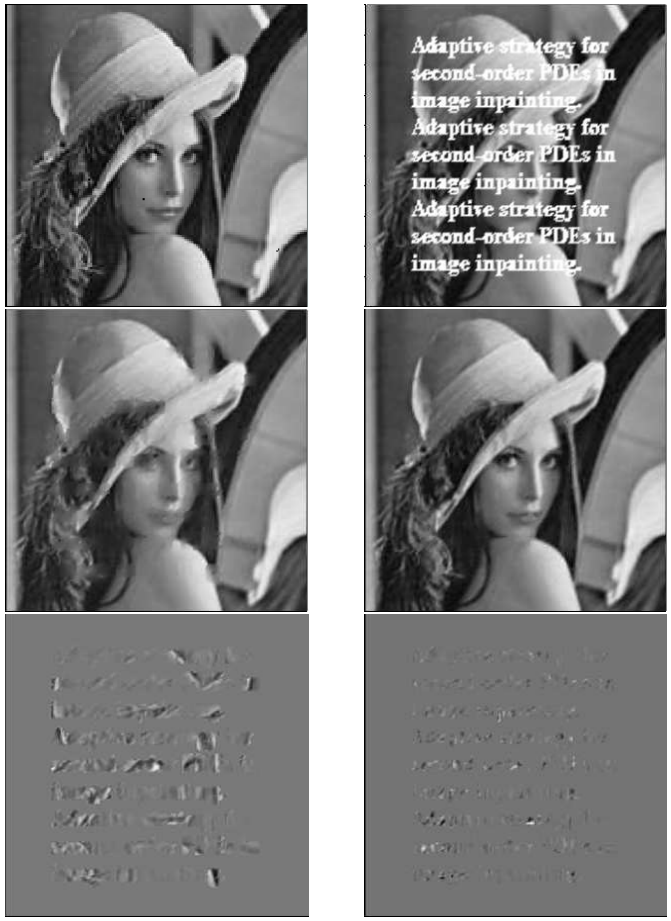

FIGURE 13. Top row: Original and damaged images. Middle row: Restored image (Harmonic & adaptation) at iterations 1 and 10, respectively. The difference between the original image and the restored one at iterations 1 and 10, respectively.

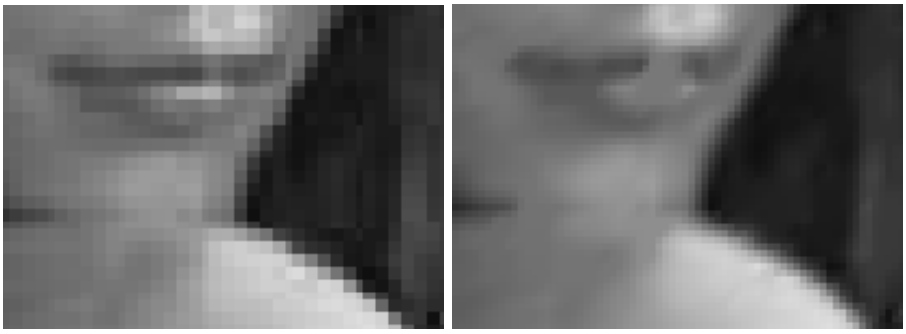

FIGURE 14. Zoom on a damaged region (40×50 Pixels): Original and restored images, respectively.

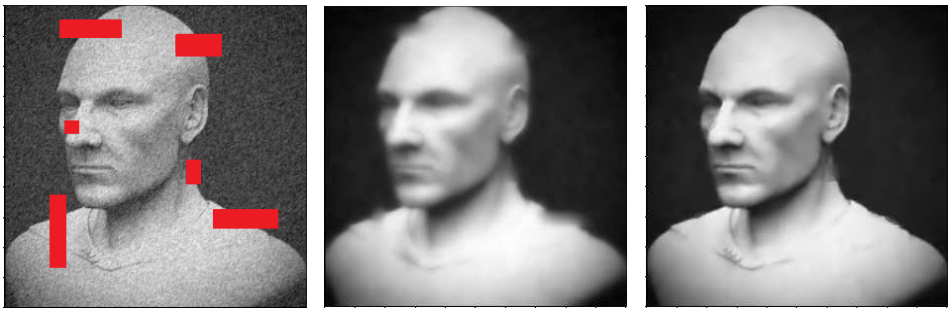

FIGURE 15. From left to right: Damaged and noisy - restored at iteration 5 - restored at iteration 20.

Examples 5. The latest example in Fig 19 deals with the reconstruction of the curvature. The inpainted edge in the missing part tends to be a straight line and it is clear that our adaptive algorithm behaves like the Mumford-Shah model (see [17] for the denoising treatment). This behavior is expected because the preferable edge with the Mumford-Shah model are those which have the shortest length due to the penalization term on the length. This example is an extreme case for second order PDEs methods which fail to capture the curvature contrary to higher order PDEs ([11]).

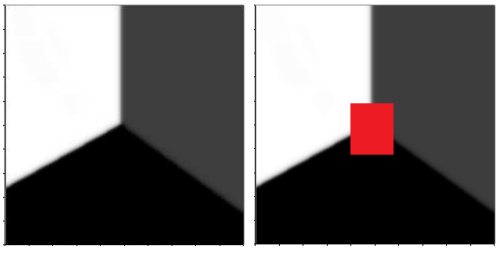

FIGURE 16. The original and damaged images.

6. Conclusion and perspectives

In this paper, we have considered an adaptive approach for image inpainting based on a local selection of the different parameters in the models, and on mesh

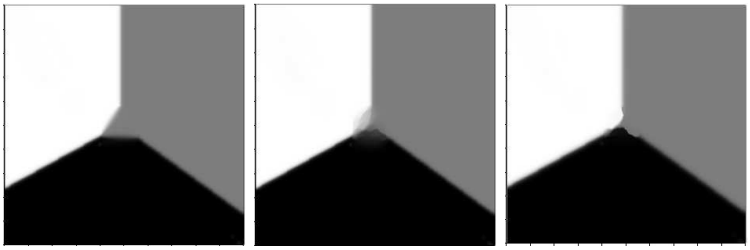

FIGURE 17. From left to right: The restored images using anisotropic nonlinear, Harmonic & adaptation and complex Ginzburg-Landau & adaptation models, respectively.

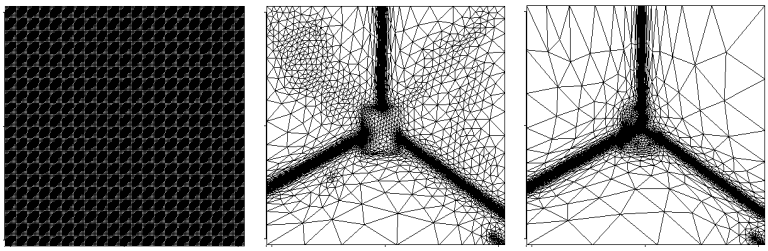

FIGURE 18. The mesh at iterations 0, 7 and 30, respectively.

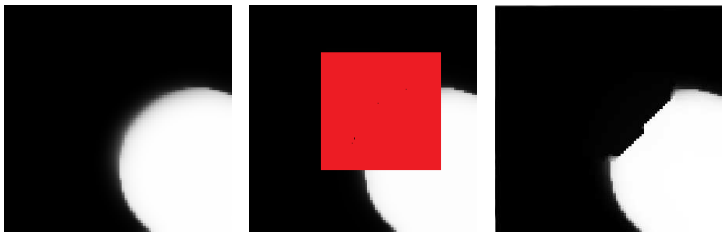

FIGURE 19. From left to right: Original, damaged and restored images (Harmonic & adaptation), respectively.

adaptation techniques. We started with the formulation of a linear variational model, and detailed its numerical implementation based on the finite element discretization which approximate in the sense of the Γ-convergence the Mumford-Shah functional. We extended the model to the Ginzburg-Landau equation, more suited for multi-gray level images. In order to make some comparisons, we presented the nonlinear diffusion model which is a standard and high quality method in image processing. The numerical experiments for the various examples presented here demonstrate the efficiency of the adaptive method and tends to confirm that finding fine structures in the reconstructed images is a matter of the diffusion more than a non-linearity in the source term in the PDE. We may say that the multi-scale strategy, based on a rigorous adaptive selection of the diffusion "rate" and location, leads to comparable results that one might expect from the nonlinear PDE considered in this field while presenting an evident advantage from the numerical point of view. Finally, the combination of this approach and the complex Ginzburg-Landau model yields very encouraging results.

The adaptive approach of the article may be applied to other problems in image analysis. Since the anisotropic diffusion remains one of the best methods, a first tentative to improve the adaptive approach is to derive an anisotropic version, which means considering α as a matrix (this is an ongoing work). A second step will be to extend it to fourth-order PDEs which are more suitable for the inpainting by preserving high curvatures ([30, 35]). Finally applying the adaptive approach to the vectorial setting (e.g. color images) would be a challenging problem and will constitute a breakthrough in the field.

References

[1] L. Ambrosio, N. Fusco and D. Pallara, Functions of bounded variation and free discontinuity problems, Oxford Mathematical Monographs, 200.
[2] L. Ambrosio and V. M. Tortorelli, On the approximation of free discontinuity problems, Boll. Un. Mat. Ital. B, 6 (1992), 105–123.
[3] G. Aubert, J. Aujol and L. Blanc-Féraud, Detecting codimension-two objects in animate with Ginzburg-Landau models, International Journal of Computer Vision, 65 (2005), 29–42.
[4] J. Aujol, T. Chan and D. Strong, Scale recognition regularization parameter selection and Meyer's G-norm in total variation regularization, Multiscale Model. Simul., 5 (2006), 273–303.
[5] D. Auroux, L.-D. Cohen and M. Masmoudi, Contour detection and completion for inpainting and segmentation based on topological gradient and fast marching algorithms, Journal of Biomedical Imaging, vol. 2011.
[6] D. Auroux and M. Masmoudi, A one-shot inpainting algorithm based on the topological asymptotic analysis, Computational & Applied Mathematics, 25 (2006), 251–267.
[7] Z. Belhachmi, C. Bernardi and A. Karageorghis, Mortar spectral element discretization of nonhomogeneous and anisotropic Laplace and Darcy equations, M2AN, 41 (2007), 801–824.
[8] Z. Belhachmi and F. Hecht, An adaptive approach for the segmentation and the TV-filtering in the optic flow estimation, Journal of Mathematical Imaging and Vision, 4/3 (2016), 358–377.
[9] Z. Belhachmi and F. Hecht, Control of the effects of regularization on variational optic flow computations, Journal of Mathematical Imaging and Vision, 40 (2011), 1–19.
[10] M. Bertalmio, A. L. Bertozzi and G. Sapiro, Navier-Stokes, fluid dynamics, and image and video inpainting, in Proc. IEEE Computer Vision and Pattern Recognition (CVPR), 2001, 355–362.
[11] M. Bertalmio, V. Caselles, S. Masnou and G. Sapiro, Inpainting, Encyclopedia of Computer Vision, Springer, 2011.
[12] M. Bertalmio, G. Sapiro, V. Caselles and C. Ballesteri, Image inpainting, in Proceedings of the 27th annual conference on computer graphics and interactive techniques, (2000), 417C424.
[13] F. Bethuel, H. Brezis and F. Helein, Ginzburg-Landau vortices, Progress in Nonlinear Differential Equations & Their Appl., Birkhäuser, Boston, MA, 1994.
[14] A. Braides, Gamma-Convergence for Beginners, 22, in Oxford Lecture Series in Mathematics and Its Applications. Oxford University Press, 2002.
[15] M. Burger, L. He and C.-B. Schnlieb, Cahn-Hilliard inpainting and a generalization for grayvalue images, SIAM J. Imaging Sci., 2 (2009), 1129–1167.
[16] F. Catté, P.-L. Lions, J.-M. Morel and T. Coll, Image selective smoothing and edge detection by nonlinear diffusion, SIAM J. Numer. Anal, 29 (1992), 182–193.
[17] A. Chambolle and B. Bourdin, Implementation of an adaptive finite-element approximation of the Mumford-Shah functional, Numer. Math., 33 (2000), 609–649.
[18] A. Chambolle and G. D. Maso, Discrete approximation of the Mumford-Shah functional in dimension two, M2AN Math. Model. Numer. Anal, 33 (1999), 651–672.
[19] T. Chan and J. Shen, Mathematical models for local non-texture inpainting, SIAM Journal on Applied Mathematics, 62 (1992), 1019–1043.
[20] T. Chan and J. Shen, Non-texture inpainting by curvature-driven diffusions, J. Visual Comm. Image Rep, 63 (2001), 564–592.
[21] G.-H. Cottet, Neural networks: continuous approach and applications to image processing, Journal of Biological Systems, 3 (1995), 659–673.
[22] G.-H. Cottet and L. Germain, Image processing through reaction combined with nonlinear diffusion, Mathematics of Computation, 61 (1993), 659–673.

[23] A. Efros and Leung, Texture synthesis by non-parametric sampling, in Proceedings of the IEEE Conference on CVPR, vol. 2 of ICCV'99, IEEE Computer Society, 1999.
[24] I. Ekeland and R. Temam, Convex analysis and variational problems, North Holland, Amsterdam, 1976.
[25] C. W. Groetsch, The theory of Tikhonov regularization for Fredholm equations of the first kind, Boston: Pitman, 1984.
[26] H. Grossauer and O. Scherzer, Using the complex Ginzburg Landau equation for digital inpainting in 2D and 3D, Scale Space Methods in Computer Vision, Lecture Notes in Computer Science 2695 (2003), 225–236..
[27] F. Hecht, New development in freefem++, Journal of Numerical Mathematics, 20 (2002), 251–265.
[28] M. Kallel, M. Moakher and A. Theljani, The Cauchy problem for a nonlinear elliptic equation: Nash-game approach and application to image inpainting, Inverse Problems and Imaging, 9 (2015), 853–874.
[29] L. Landau and V. Ginzburg, On the theory of superconductivity, Journal of Experimental and Theoretical Physics (USSR), 20 (1950), 1064..
[30] S. Masnou, Disocclusion: a variational approach using level lines, IEEE Transactions on Image Processing, 11 (2002), 68–67.
[31] V. A. Morozov, Methods for solving incorrectly posed problems (translation ed.: Z. Nashed), Wien, New York: Springer, 1984.
[32] M. Nitzberg and T. Shiota, Nonlinear image filtering with edge and corner enhancement, IEEE Transactions on Pattern Analysis and Machine Intelligence, 14 (1992), 826–833.
[33] P. Perona and J. Malik, Scale-space and edge detection using anisotropic diffusion, IEEE Transactions on Pattern Analysis and Machine Intelligence, 12 (1990), 629–639.
[34] T. Schoenemann, S. Masnou and D. Cremers, On a linear programming approach to the discrete Willmore boundary value problem and generalizations, in Curves and Surfaces, vol. 6920 of Lecture Notes in Computer Science, Springer Berlin Heidelberg, 2012, 629–646.
[35] J. Shen, S. H. Kang and T. Chan, Euler's elastica and curvature-based inpainting, SIAM J. Imaging Sci., 63 (2002), 564–592.
[36] D. Strong, Adaptive total variation minimization image restoration, PhD thesis, UCLA Mathematics Department, USA, 1997.
[37] R. Verfurth, A Review of a Posteriori Error Estimation and Adaptive Mesh-Refnement Techniques, Wiely & Teubner, 1996.
[38] J. Weickert, Theoretical foundations of anisotropic diffusion in image processing, Theoretical Foundations of Computer Vision Computing Supplement, 11 (1996), 221–236.

Mathematics, Information Technology and Applications Laboratory, University of Haute Alsace, France.
E-mail: zakaria.belhachmi@uha.fr

IPEIT, Université de Tunis, 2, Rue Jawaher Lel Nehru, 1089 Montfleury, Tunisia.
E-mail: moez.kallel@ipeit.rnu.tn

National Engineering School at Tunis, University of Tunis-El Manar, B.P. 37, 1002 Tunis-Belvédère, Tunisia.
E-mail: maher.moakher@gmail.com

LAMSIN-ENIT, University of Tunis-El Manar, B.P. 37, 1002 Tunis-Belvédère, Tunisia.
E-mail: thaljanianis@gmail.com